Novel Lysine-Rich Delivery Peptides of Plant Origin ERD and Human S100: The Effect of Carboxyfluorescein Conjugation, Influence of Aromatic and Proline Residues, Cellular Internalization, and Penetration Ability

Fanni Sebák, Lilla Borbála Horváth, Dániel Kovács, János Szolomájer, Gábor K. Tóth, Ákos Babiczky, Szilvia Bősze, and Andrea Bodor*

ACCESS | Metrics & More | Article Recommendations | SI Supporting Information

ABSTRACT: The need for novel drug delivery peptides is an important issue of the modern pharmaceutical research. Here, we test K-rich peptides from plant dehydrin ERD14 (ERD-A, ERD-B, and ERD-C) and the C-terminal CPP-resembling region of S100A4 (S100) using the 5(6)-carboxyfluorescein (Cf) tag at the N-terminus. Via a combined pH-dependent NMR and fluorescence study, we analyze the effect of the Cf conjugation/modification on the structural behavior, separately investigating the (5)-Cf and (6)-Cf forms. Flow cytometry results show that all peptides internalize; however, there is a slight difference between the cellular internalization of (5)- and (6)-Cf-peptides. We indicate the possible importance of residues with an aromatic sidechain and proline. We prove that ERD-A localizes mostly in the cytosol, ERD-B and S100 have partial colocalization with lysosomal staining, and ERD-C mainly localizes within vesicle-like compartments, while the uptake mechanism mainly occurs through energy-dependent paths.
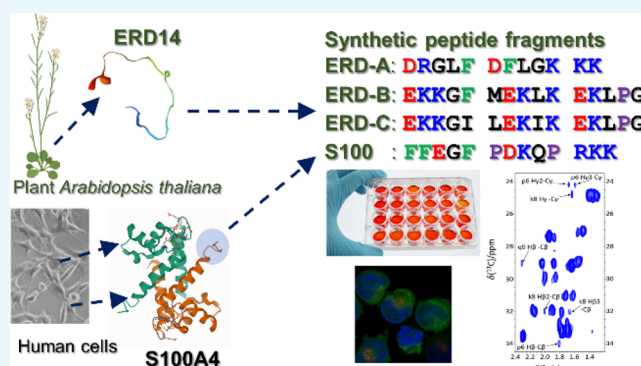
INTRODUCTION

Drug delivery through the cell membrane continues to be an important issue of modern pharmaceutical research. In this respect, application of cell-penetrating peptides (CPPs) is a promising tool to achieve enhanced drug delivery for antitumor treatment. CPPs are short (usually less than 30 amino acids), positively charged peptides with amphipathic characteristics, capable of rapidly entering cells without cytolytic effects. The requirements toward these constructs are good water solubility and biocompatibility. The first and most extensively studied CPPs are the human immunodeficiency virus type 1 (HIV-1)-encoded TAT peptide[1,2] and the amphiphilic *Drosophila* Antennapedia homeodomain-derived 16 amino acid penetratin.[3,4] A serious issue is that several CPPs interact with the cell membranes, causing unwanted cytotoxic effects.[5] Thus, development of better and better candidates for drug delivery is needed. Bioactive peptides of plant origin can present an alternative, and several biological effects (e.g., antimicrobial or signaling peptides and development regulation) of plant-derived peptides were already described.[6] Also, these peptides are safer for human application due to the lack of animal-derived substances and less allergenic and cytotoxic effects. Being safe and selective, they can be applied as ingredients in dietary supplements and pharmaceutical or cosmetic products and used as wound-healing, skin care, and anti-aging agents. On the other hand, the eco-friendly ingredients of plant origin are more and more popular as strict vegan customers are an increasing market.[7] Interest toward such biomolecules is increasing, and recently, a manually curated database of plant-derived peptides with different functions and therapeutic activities has been assembled (PlantPepDB: http://www.nipgr.ac.in/PlantPepDB/).[8] In this respect, our aim was to focus on Lys-rich regions from plant dehydrin ERD14 (denoted ERD-A, ERD-B, and ERD-C) and the C-terminus of the Ca^{2+}-loaded, homodimeric metastasis-associated S100A4 (denoted S100).

ERD14 dehydrin is a 185 residue-long, disordered plant stress protein from *Arabidopsis thaliana* and contains several conserved segments.[9] The lysine-rich segments (so-called K-

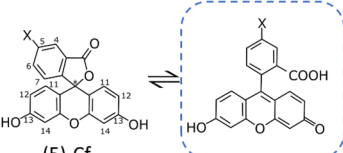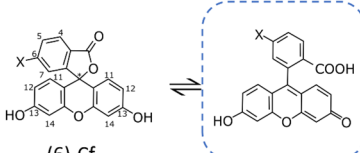**Scheme 1. (A) Sequence of the Lysine-Rich Peptides, pI, and Charge at Different pH Values; (B) Two Tautomeric Forms of (5)- and (6)-Cf**[a]

Peptide	Code	Length	Sequence	pI	Charge at pH 3.0	Charge at pH 5.0	Charge at pH +7.0
ERD14 K A	ERD-A	12	DRGLF DFLGK KK	9.7	+4.5	+2.4	+1.9
ERD14 K B	ERD-B	15	EKKGF MEKLK EKLPG	9.4	+5.4	+2.6	+1.9
ERD14 K C	ERD-C	15	EKKGI LEKIK EKLPG	9.4	+5.4	+2.6	+1.9
S100A4 C-terminus	S100	13	FFEGF PDKQP RKK	9.7	+4.5	+2.4	+1.9

[a]At neutral pH, the carboxylic acid is the main tautomer for both forms (highlighted).

segments) contribute to the chaperone activity and cell viability under stress. These regions show a nascent helical propensity, while the full-length ERD14 is disordered.[10,11] In the case of different plant dehydrins (DHN1 and Lti30), K-segments were identified as the interaction site with anionic lipid bilayers.[12,13] In-cell nuclear magnetic resonance (NMR) measurements show that the signals of the K-segments are broadened below the detection limit that can be a consequence of protein/protein, protein/DNA or protein/membrane interaction.[14,15]

Furthermore, the human carrier peptide candidate is the C-terminal part of the metastasis-associated S100A4 protein, where the C-terminal segment resembles mainly ERD-A, but the hydrophobic residue pattern differs.

The homodimeric, Ca^{2+}-binding human S100A4 is a 101 residue-long protein involved in cancer progression, invasiveness, and metastasis.[16,17] Fifteen C-terminal amino acids are responsible for S100A4-induced metastasis and cell migration.[18,19] S100A4 is able to penetrate the cell membrane with an energy-dependent endocytic pathway;[20] however, it remains uncertain which region is responsible for the phenomenon.

All these peptides (ERD- and S100A4-derived) share sequential similarity to the widely studied CPPs, such as penetratin (RQIKIWFQNRRMKWKKGG), with several cationic residues separated by hydrophobic amino acids[21] (sequence and charges are collected in Scheme 1A), and according to prediction analysis, they can act like CPPs (Table S1).[22] On the other hand, previous studies already discussed the membrane-associative properties of these segments, emphasizing their biological relevance.[9,14,18,20] As shown on Scheme 1A, our studied peptides harbor differently distributed Lys residues; ERD-A and S100 have three lysines, out of which the C-terminus is KK, while ERD-B and ERD-C have five lysines in identical positions, with the KK motif at the N-terminus and the other residues uniformly distributed along the sequence. The electric charge at physiological pH for all studied peptides is the same (+1.9); at pH = 3, ERD-B and ERD-C have somewhat higher positive charge (+5.4) compared to +4.5 for ERD-A and S100.

To perform *in vitro* cell penetration studies, a fluorescent moiety is usually conjugated to the peptides, which enables indirect quantification and visualization by confocal microscopy inside living cells. Fluorophores are generally hydrophobic small molecules and the most common choice in peptide chemistry is 5(6)-carboxyfluorescein (Cf, Scheme

1B).[23] Cf has good solubility in solvents used in peptide synthesis (*N,N*-dimethylformamide, DMF; 1-methylpyrrolidin-2-one, NMP), and it can be coupled easily to the peptide chain via an amide bond between the Cf carboxyl group and the free N-terminal amine group of the peptide (N or sidechain of a Lys).[24] The commercially available Cf is usually a mixture of two isomers: (5)-Cf and (6)-Cf; consequently, peptides will be attached to these positions, and during the purification step, these isomers are not separated. However, the conjugated fluorescent moiety can alter the physicochemical properties (lipophilicity), the conformation, and the flexibility of the peptide; consequently, the penetration, internalization ability, intracellular localization, and cytotoxicity can/will be affected. Comparing the *ex vivo* and *in vitro* penetration ability of seven cationic peptides, Kiss *et al.* indicated that the Cf tag changes the peptide lipophilicity and penetration ability through *ex vivo* membrane models.[25] The coupling of the Cf moiety at the N-terminus introduces asymmetry in polarity, possibly rendering these peptides more amphiphilic.[25] In a study of Szeto *et al.*, in the DALDA tetrapeptide (Dmt-D-Arg-Phe-Lys-NH$_2$, where Dmt is 2′,6′-L-dimethyltyrosine), lysine amino acid was replaced with two different fluorescent moieties.[26] A dansyl-containing fluorescent analog was located in the mitochondrial matrix instead of localization in the inner mitochondrial membrane.[26] TAT and penetratin cytotoxicity was lower if used as a nonfluorescent derivative or with a small cargo compared to when used with a larger cargo.[27] In a comparative study of seven fluorophores conjugated to the N-terminus of penetratin, Birch *et al.* identified relations between the chemical characteristics and the impact on the *in vitro* cytotoxic effect.[28] The neutral or negatively charged fluorophores had a lower cytotoxic effect than the positively charged fluorophores.[28] Cavaco *et al.* compared the effect of four fluorescent moieties conjugated to the N-terminus of four model peptides, and based on this study, 5(6)-Cf has no effect on the peptide cytotoxicity.[29] Hughes *et al.* carried out a systematic study on different water-soluble, commercially available dyes to compare the interaction ability between fluorescent dyes and model lipid bilayers. They observed that Cf has remarkably weak association with lipid bilayers.[30] Their findings make the Cf an optimal peptide conjugate fluorophore to investigate the cellular uptake of carrier peptide candidates.

The most common methods to monitor the effect of fluorophores on the peptide structure are circular dichroism (CD) and computational prediction.[25,31,32] However, a tool
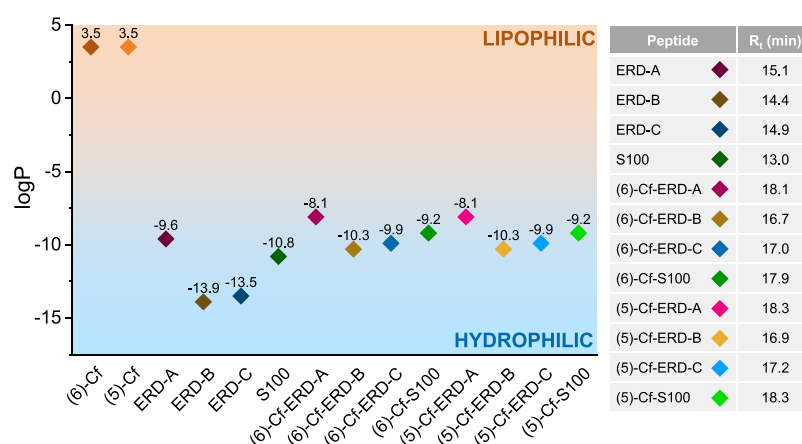
Figure 1. Lipophilicity of peptides and Cf-peptides. Retention times were determined using an Exforma EX1600 analytical HPLC with a YMC-Pack ODS-A C18 (100 Å, 4.6 × 150 mm) column. Flow rate: 1 mL/min; detector: λ = 220 nm; gradient: 0−20 min, 5−65 B%. A eluent: 0.1% (v/v) TFA in ddH$_2$O; B eluent: 0.1% (v/v) TFA in acetonitrile:H$_2$O (80:20, v/v).

that can be very sensitive to conformational and structural changes is NMR spectroscopy. Even at a low peptide concentration, modern pulse sequences allow, besides the usual ^{1}H-^{1}H homonuclear correlations, acquisition of ^{1}H-^{13}C and ^{1}H-^{15}N heteronuclear spectra in feasible experimental times. Thus, an in-depth characterization of several atomic environments reporting on structural propensities becomes available. The variation of these parameters with pH can be relevant considering the possible localization of peptides in the different cellular compartments, which, due to different pH values, will affect the fluorescence properties.

Therefore, in the present study, we proposed to test the cell-penetrating properties of the K-rich domains of ERD14, as well as the C-terminal S100A4 fragment. To determine whether there is any difference between the (5)- and (6)-substituted Cf fragments, we analyzed separately both forms via a thorough NMR methodology and characterized the structural differences that might affect the biological behavior.

Further, for these peptides, we investigated the cellular uptake, the intracellular localization on A431 skin squamous cell carcinoma cell lines, the cytotoxic activity, and the effect of different inhibitors on the cellular uptake.

RESULTS

Synthesis and Characterization of Peptide Derivatives. The four designed peptides (Scheme 1A) were synthesized using solid-phase peptide synthesis, applying the Fmoc/tBu strategy using a CEM microwave-assisted fully automated peptide synthesizer. Due to its good solubility, easy application, low cytotoxic effect, and negligible interaction with the cell membrane, the 5(6)-carboxyfluorescein (Cf) fluorophore was selected and conjugated to the peptides. The crude products were purified using a C18 RP-HPLC on a PerfectSil 100 ODS-3 5 μm (250 × 10 mm) column. In most cases, the two regioisomers (5)-Cf and (6)-Cf were well separable on the RP-HPLC column, and an isomeric ratio of 80:20 could be achieved during purification. Purified products were identified by analytical HPLC, mass spectrometry, and amino acid analysis. The calculated monoisotopic masses, measured masses, retention times, and amino acid content are presented in Table S2 and Figures S1−S3. In all cases, measured masses coincided with the calculated value and a purity of at least 95% was detected.

A crucial parameter to test is peptide lipophilicity. Lipophilic molecules (e.g., fluorophores and small molecule drugs) conjugated to the peptides decrease the hydrophilicity of the carriers. It is important that upon conjugation, such lipophilic moieties do not significantly alter the water solubility of the carrier peptides. Calculated log$P$ values of the peptides and Cf-peptide derivatives (Figure 1) were determined using the Chemicalize online platform (https://chemicalize.com/) developed by ChemAxon (http://www.chemaxon.com) (see Determination of Lipophilicity Profile of the Peptides and Their Cf Conjugates). Based on the calculated log$P$ values, ERD and S100 peptides are hydrophilic. Upon conjugation of Cf to the N-terminus, log$P$ values become more positive, as expected; thus, Cf-peptide derivatives are more lipophilic than the original peptides. The mostly hydrophobic ERD-A and S100 will have a small increase in log$P$ (1.5 and 1.6, respectively), while ERD-B and ERD-C will show an increase of 3.6. Still, even with these shifts, log$P$ values are well <0 and show good solubility in the aqueous phase. Overall, the studied peptides are optimal candidates as carriers of even extremely lipophilic drug candidates.

pH-Dependent NMR Properties and Fluorescence Intensity of Cf and Cf-Peptide Derivatives. A disadvantage of the commonly used Cf fluorophore is its pH-dependent fluorescence intensity, which is significantly lower under acidic conditions compared to neutral conditions, due to the equilibrium between the two tautomeric forms (Scheme 1A).[33] The literature suggests that the nonfluorescent lactone tautomer is predominant in aprotic solvents and in acidic aqueous solutions.[34] In contrary, the carboxylic acid form is expected to dominate in protic solvents and, thus, in both neutral and alkaline aqueous solutions, where the more expanded π-electron system is responsible for the increased fluorescence.

NMR spectroscopy enables both the determination of the tautomeric forms of Cf and the shift of the tautomeric equilibrium with pH/solvent. The dimethyl sulfoxide (DMSO) solvent shifts the equilibrium toward the lactone form, while the carboxylic acid form is predominant in alkaline media. To decide which form is present, C*, C^{13}, and C^{12} are the key atoms (see Scheme 1B). In the lactone form, the C* carbon has sp^3 hybridization. In DMSO, the ^{1}H,^{13}C-HMBC measurement shows a ^{1}H^{11}−^{13}C* correlation with a C* chemical shift

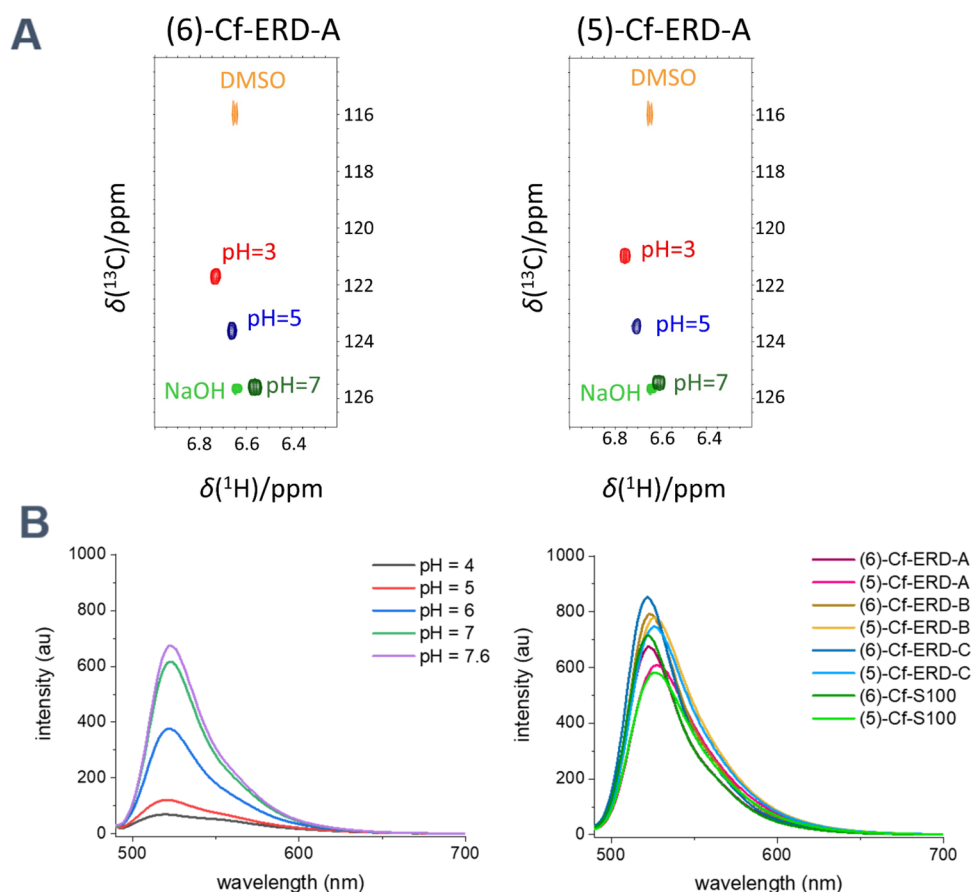**Figure 2.** (A) Overlay of the $^1H,^{13}C$-HSQC spectra showing the $H^{12}–C^{12}$ cross-peak under different conditions; (B) fluorescence emission spectra of the (6)-Cf-ERD-A peptide in different pH value buffers and Cf-peptides at pH = 7.6. Excitation: λ = 488 nm; emission: λ = 490−700 nm; detector voltage: 450 V; peptide concentration: 6.25 μM.

of 86.6 ppm in accordance with the sp^3 hybridization state detected for both (5)- and (6)-Cf. In a 25 mM NaOH medium, the $^1H,^{13}C$-HMBC measurement shows the $^1H^{11}–^{13}C^*$ correlation that is missing in the 86.6 ppm region (Table S3). The carboxylic acid form should present a correlation in the aromatic region; unfortunately, due to signal overlap, this correlation is not distinguishable from the other aromatic peaks. However, the $^1H^{11}–^{13}C^{13}$ correlation shows a shift of the $\delta(C^{13})$ from 162 ppm (in DMSO) to 184 ppm, while in the $^1H,^{13}C$-HSQC spectra, the $^1H^{12}–^{13}C^{12}$ correlation shifts from 115 ppm to 125.6 ppm (Figure 2A). These changes can be attributed to the opening of the lactone ring, causing the phenolic C^{13}-OH environment to shift toward a $C^{13}{=}O$ form, with the carbon atoms becoming more deshielded. Thus, the C*, C^{13}, and C^{12} chemical shifts are worthwhile to follow upon monitoring the lactone/carboxylic acid equilibrium. Measurements of (5)- and (6)-Cf peptides at different pH values show that the C* at 86.6 ppm is missing, while C^{13} and C^{12} have values between the detected extremes, slightly closer to the higher value, indicating that the equilibrium is shifted to the carboxylic open form (see Figure 2A and Table S3), and at around pH = 7, the carboxylic tautomer is present almost exclusively. These experiments highlight that through the alternation of Cf and the tautomeric equilibrium, the intracellular pH values affect both the polarity and the fluorescence properties of the fluorophore.

The fluorescence properties of Cf can be affected by the attached peptide and they have great importance in the proper

comparison of the cellular uptake rates of Cf peptides. Therefore, prior to the cellular uptake studies, the pH dependence of the fluorescence intensity of the Cf-peptide derivatives was studied in citric acid−Na$_2$HPO$_4$ buffers in the 4.0−7.6 pH range, representing intracellular pH values of different cellular compartments.[35] For all peptides, a strong pH dependence is observed: the more acidic the pH, the lower the fluorescence intensity, while between pH = 7.0−7.6, no significant increase in the fluorescence intensity occurs (Figure 2B and Figures S4 and S5). On the other hand, the peptide amino acid sequence has only a moderate effect on the fluorescence intensity, as seen from the emission spectra of all Cf peptides at pH = 7.6 (Figure 2B and Figure S5). These results are in full accordance with the outcome of the above-discussed NMR experiments.

Cellular Internalization of Cf-Peptides and Their Effect on Cell Viability. The cellular uptake was quantified by flow cytometry, and several sets of preliminary experiments were performed to optimize the experimental conditions (concentration range, incubation times, etc.; see Figures S9–S13). To determine the internalization cellular uptake profile, the Cf peptides were studied on A431 human skin squamous cell carcinoma cells. Cells were treated with the (6)-Cf and (5)-Cf peptides in the 0.2−25 μM concentration range for 90 min. Three independent experiments were performed. Cell viability during flow cytometry was evaluated using the propidium iodide (PI) exclusion-based gating strategy. Cf peptides have no cytotoxic effect on A431 cells as the relative
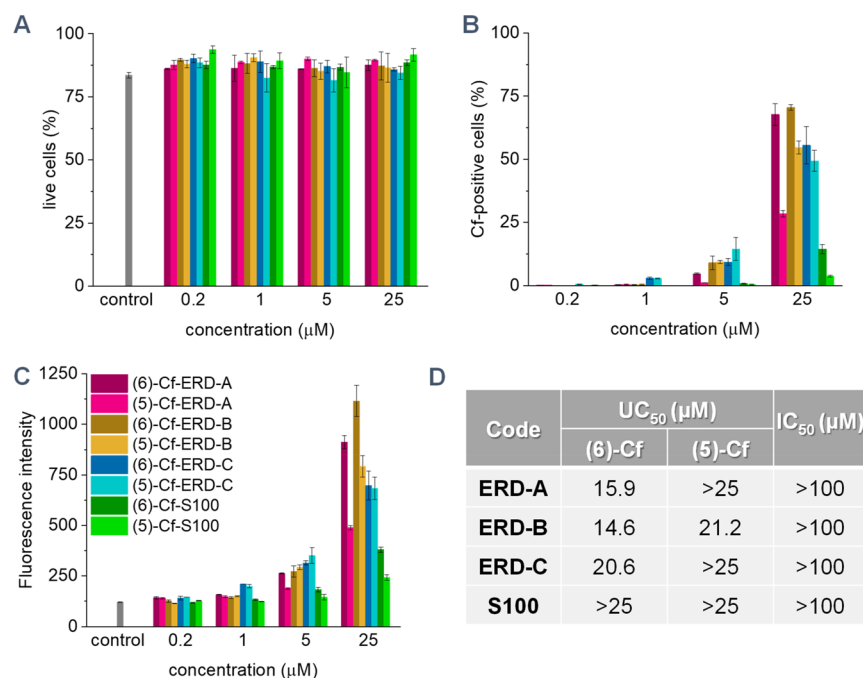
Figure 3. *In vitro* cellular uptake of the synthetic Cf-peptides on A431 cells quantified by flow cytometry. Treatment conditions: concentration range, 0.2−25 μM; 90 min. (A) Relative viability of A431 cells compared to untreated control. Cellular uptake of the Cf peptides: (B) ratio of Cf-positive live cells and (C) mean fluorescence intensity. Error bars correspond to SEM (standard error of the mean). (D) A quantified value of the Cf peptide uptake rate, UC$_{50}$ (concentration of compounds where the rate of fluorescence positive cells reaches 50%), can be drawn from the ratio of fluorescence-positive cells at different concentrations and IC$_{50}$ values of the peptides.
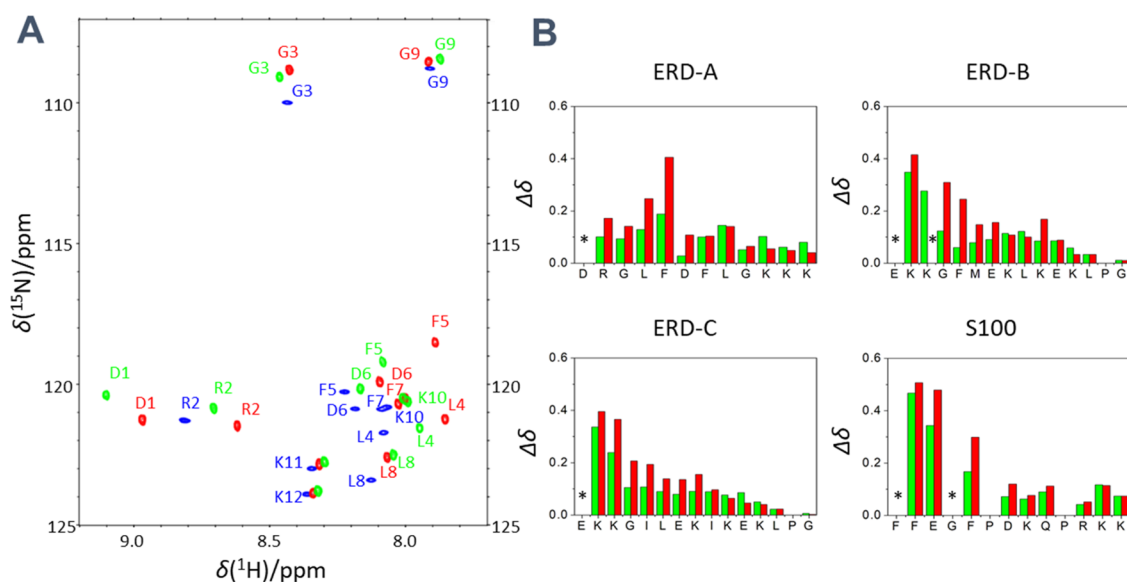

Figure 4. (A) Overlay of the natural isotope abundance ^{1}H,^{15}N-SOFAST-HMQC spectra of ERD-A peptides at pH = 3: nonfluorescent (blue), (5)-Cf (green), and (6)-Cf variant (red). (B) $\Delta\delta$ chemical shift difference values for the studied ERD and S100 peptides at pH = 3. The asterisks (*) highlight residues with increased exchange, which are undetectable in the spectra.

viability is similar for both treated and untreated cells during all experiments (Figure 3A). The relative viability of the cells was above 80% for each Cf peptide.

In all cases, concentration-dependent cellular uptake is observed, characterized by the enhanced intracellular fluorescence (Figure 3B, C); however, significant differences between the cellular uptake of peptides have been observed. For all concentrations, S100 has the lowest cellular uptake rate. While at 1 and 5 μM concentrations of ERD-C, at 25 μM, ERD-B has the highest cellular uptake. These tendencies are confirmed both by the ratio of Cf-positive cells and the mean fluorescence intensity. It is interesting to note that a significant difference is detected between the Cf isomers: for (6)-Cf-ERD-A, the cellular uptake is more than two times higher than for (5)-Cf-ERD-A at 25 μM concentration (Figure 3B). For ERD-B and ERD-C, the difference also exists, but it is slightly lower. For all peptide derivatives, the (6)-Cf isomers have higher cellular uptake. In the case of (6)-Cf-S100 and (5)-Cf-S100 peptides, also a significant difference can be detected; (6)-Cf-
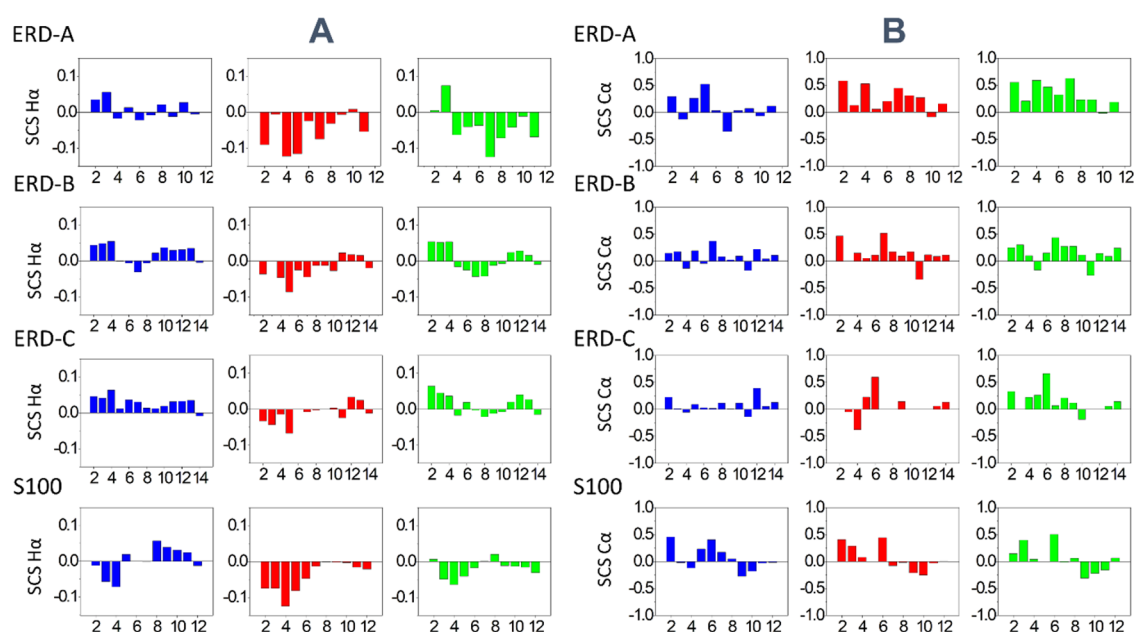
Figure 5. Secondary chemical shift values along the amino acid sequence calculated from (A) measured Hα and (B) Cα chemical shifts for nonfluorescent (blue), (6)-Cf (red), and (5)-Cf-conjugated (green) ERD-A, ERD-B, ERD-C, and S100 peptides.

conjugated peptides have higher cellular uptake than (5)-Cf isomer-conjugated peptides.

Further, the corresponding UC$_{50}$ values—the interpolated concentration required for intracellular fluorescence in 50% of the cells—were calculated as described earlier[36] (Figure 3D). For both Cf isomers, ERD-B has the lowest value, meaning the highest cellular uptake. ERD-A and ERD-C peptides have similar cellular uptake. The S100 peptide has the lowest cellular uptake to A431 cells. On the other hand, the (6)-Cf isomers show lower UC$_{50}$ values.

Parallel with the flow cytometry measurements, we have also determined the *in vitro* cytostatic activity of non-Cf-conjugated peptides using the MTT assay. Cells were treated with the peptides in the concentration range of 1.28×10^{-3} to 100 μM for 20−24 h. After washing, cells were incubated for 72 h. The MTT assay was performed after the incubation. Figure 3D summarizes the 50% inhibitory concentration (IC$_{50}$) values—the concentration required for inhibiting the growth of 50% of the cells. No cytostatic effect was observed in this concentration range.

NMR Studies Reveal the Effect of Cf Conjugation on the Different Atomic Environments and the Importance of the Peptide Amino Acid Sequence. The cellular uptake of (5)- and (6)-Cf-peptides proved to be different; therefore, we proposed to analyze possible reasons for this behavior. As such, we investigated whether the presence of the aromatic ring in the Cf moiety causes any conformational changes in the studied peptides, moreover, if the amino acid sequence of the peptide has any influence. In this respect, changes in the atomic environments are useful parameters, and we performed full ^{13}C, ^{1}H, and ^{15}N spectral assignment from homonuclear and heteronuclear correlations at natural isotope abundance. Further, backbone −NH− moieties from the ^{1}H,^{15}N-SOFAST-HMQC spectra[37] (Figure 4 and Figure S6) of the nonfluorescent and Cf conjugates were compared, and in the case of each peptide, a slight change for most residues has been observed. To quantify this effect, Δδ values were calculated

using the ^{1}H and ^{15}N chemical shifts based on the following equation[38] (Figure 4B) (eq 1):

$$\Delta\delta = \sqrt{(\delta_{H_1} - \delta_{H_2})^2 + (0.1(\delta_{N_1} - \delta_{N_2}))^2} \qquad (1)$$

where 1 represents the chemical shift values for the Cf conjugates, and 2 represents those for the nonfluorescent peptide at the same pH.

Δδ plots indicate that (6)-Cf has a bigger effect, and as expected, in most cases, the N-terminal region is affected by shifts gradually decreasing along the peptide sequence. Still, it is surprising that the disturbance caused by the presence of the introduced fluorescent moiety is felt quite far along the peptide backbone (at least for a 6−7 residue-long segment). This decay is uniform for ERD-B and ERD-C peptides, where values drop starting from 0.4, and for the (6)-Cf peptides, the values are ∼0.1 higher. For S100 even at the C-terminus, a small disturbance is felt, and as this sequence contains two Pro residues without amide H, no values are determined. For ERD-A, the perturbation on the N-terminus is not as pronounced. It is interesting to see which amino acids affect this behavior. In all peptides except ERD-C, Phe residues occur in position 5. This residue for the (6)-Cf peptide has high ∼0.4 values, while for the (5)-Cf peptide at this position, the perturbation significantly lowers (the difference is at least 0.2). For ERD-C, position 5 is occupied by Ile, with a 0.2 perturbation value. On the other hand, the Phe residue in the N-terminus of S100 is >0.4 compared to other non-aromatic N-terminal amino acids. Also, where possible, the residues in the Phe neighborhood have more accentuated differences between the (5)- and (6)-Cf-conjugated peptide forms. All these results indicate that besides the different Cf isomers, also aromatic residues affect the positions of the −NH− backbone moieties; in their absence, a uniform decay is observed (as seen for ERD-C).

Further, to monitor structural changes caused by the Cf conjugation/modification, we calculated corresponding secondary chemical shifts (SCSs) (Figure 5) (eq 2):

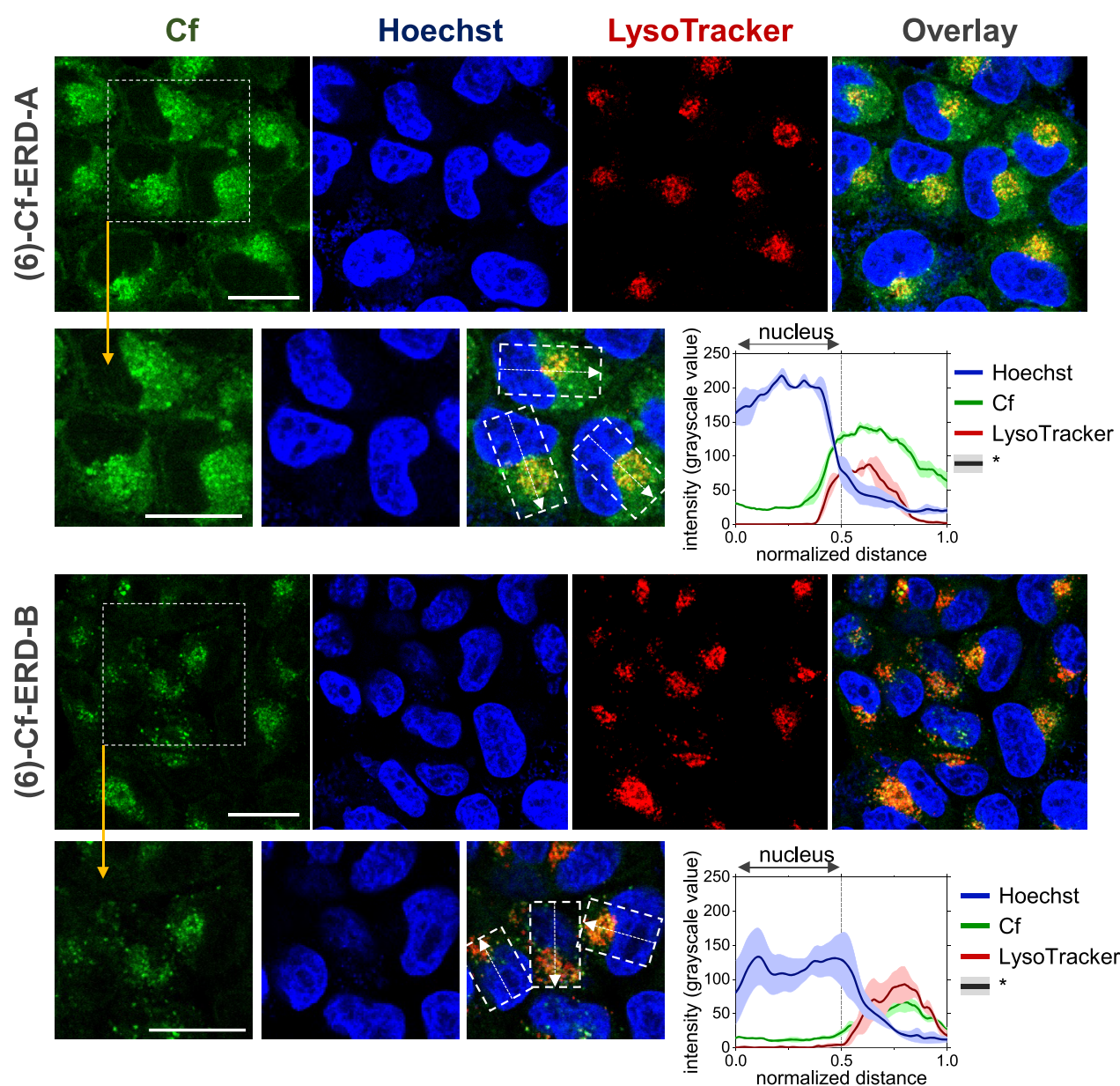$$SCS = \delta_{measured} - RCCS \qquad (2)$$

Figure 6. *In vitro* intracellular localization of Cf-peptides visualized by CLSM. Cells were treated for 90 min with Cf peptides (25 μM, green). Lysosomes were stained by LysoTracker Deep Red (red), and nuclei were stained by Hoechst 33342 (blue). Imaging was performed by the Zeiss LSM 710 system; scale bars represent 20 μm. The asterisks (*) indicate that the standard error was calculated and visualized by OriginPro 2018 software.

where RCCS is the random coil chemical shift for the given residue and its value was obtained from the POTENCI web server approach (using pH and temperature corrections).[39]

As expected for these short peptides, the SCS analysis reveals no stable secondary structure regardless of the presence or absence of any of the labels. Both SCS Cα and Hα are consensual in this aspect; nevertheless, slight changes in the structural propensities can be detected. All peptides become more helical with Cf conjugation, and (5)- and (6)-Cf-ERD-A show the most helical propensities (with SCS Hα-negative and SCS Cα-positive tendencies over several residues, although the values are low, showing no formation of a real helix). For ERD-C, Cf conjugation still points to the direction of obtaining a slight helical character.

A closer analysis of the S100 peptide spectra reveals peak multiplication around the Pro6 residue. The appearing minor peaks are a consequence of the *cis/trans* Pro isomerization, occurring spontaneously in solution. Minor peak intensities can be quantified using the equation [minor] = [minor]/([major] + [minor]) $\times$ 100%, and a 25% content is obtained, in full agreement with the behavior of Pro-containing, short, disordered peptides.[40,41] To unambiguously prove the Pro isomeric form, Cβ-Cγ chemical shifts were determined. The δ(Cβ) = 33.93 ppm and δ(Cγ) = 24.18 ppm values indicate that minor Pro6 has *cis*-conformation[42] (Figure S6D). This has structural consequences, as a turn in the secondary propensity of the minor conformer will be formed, causing an even more heterogeneous conformational ensemble for the disordered peptide, possibly with lower penetration ability. The actual process of internalization mainly depends on the physico-chemical (length, net charge, log$P$, etc.) and structural properties of the peptide (and the actual cargo as well as the

concentration applied) in combination with the properties of the cell membrane.[43]

ERD-B and ERD-C peptides have Pro at the C-terminus; a peak multiplication of the neighboring residues is also detectable, but being already the mobile end, these fragments' proline position will influence less the cell penetration properties.

To mimic a range of cellular microenvironments, various spectra of (5)-Cf, (6)-Cf-ERD-A, and (6)-Cf-ERD-B were recorded at pH values of 3, 5, and 7. The $^{1}H,^{15}N$-SOFAST-HMQC spectra exhibit pH-dependent signals due to the H^{+} exchange between the dissociable −NH− environments and water. The $^{1}H,^{13}C$-HSQC spectra, being much more descriptive of the secondary structural state of the peptide, are essentially unchanged in the examined pH range (Figures S7 and S8). In this case, the only pH-dependent signals belong to glutamic acid residues. This pH sensitivity is an effect of the titratability of the sidechains and cannot be attributed to structural changes. These results indicate that in this pH range, no changes occur in the structural propensities; thus, localization into cytosol or liposomes will not alter this behavior.

Investigation of spatial proximities induced by the presence of the Cf modification was done by the $^{1}H-^{1}H$ NOESY spectra. Cross-peaks are detected between protons that are close in space (<5 Å), and in our disordered peptides, mostly sequential ($i, i − 1$) peaks are observed. In some cases, although Cf is involved in minor interaction with the Phe sidechains, (6)-Cf-ERD-A Phe5 sidechain protons (HD and HE) are close to Cf H^{7} and H^{14}; furthermore, cross-peaks between Phe7 HZ and H7 are also detected. For (5)-Cf-ERD-A and ERD-B variants, the NOE pattern is similar. This obviously means an alteration of the original conformational ensemble and offers a potential explanation to both increased SCS and $\Delta\delta$ values.

Intracellular Localization of Cf-Peptides Using Confocal Laser Scanning Microscopy. Next, we analyzed the intracellular fate of the new Cf-peptide variants using confocal laser scanning microscopy (CLSM) at the 25 μM Cf-peptide concentration (based on the flow cytometry profile), and A431 cells were incubated for 90 min. Representative images are presented in Figures 6 and 7. No colocalization with nuclei staining can be observed, proved also by the line scan analysis of (6)-Cf-ERD-A and (6)-Cf-ERD-B (Figure 6). According to the fluorescent signals, the peptide (6)-Cf-ERD-A is mainly
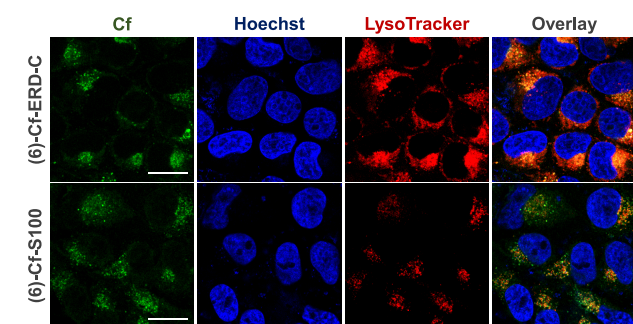

Figure 7. *In vitro* intracellular localization of Cf-peptides visualized by CLSM. Cells were treated for 90 min with Cf-peptides (25 μM, green). Lysosomes were stained by LysoTracker Deep Red (red), and nuclei were stained by Hoechst 33342 (blue). Imaging was performed by the Zeiss LSM 710 system; scale bars represent 20 μm.

localized in the cytoplasm, while the peptide (6)-Cf-ERD-B is also accumulated in the cytosol and partially colocalized with lysosomal staining. The peptide (6)-Cf-ERD-C mainly accumulated in lysosomal compartments (based on lysosomal staining). In the case of the peptide (6)-Cf-S100, partial colocalization with lysosomal staining was observed. Colocalization with lysosomal staining can indicate vesicular transport involved in the uptake of Cf peptides. (5)-Cf peptides have similar *in vitro* intracellular localization as (6)-Cf peptides. (All microscopy images are presented in Figures S14−S17, Supporting Information.)

Analyzing the internalization process is essential in the case of peptides to develop carriers with high selectivity (low cytotoxicity) and cell specificity. The length, charge distribution, and conformation guide the internalization paths of the carrier peptides to two major routes: endocytosis (energy-dependent or active internalization) and direct membrane translocation (energy-independent or passive internalization) in combination with the properties of the cell membrane. Endocytosis is a complex process composed of different steps. The direct translocation as a single-step process of peptides through the cell membrane is an alternative to endocytosis, which was suggested at a low temperature (Figure 8A based on refs[43] and[44]).

To investigate the process of the cellular internalization, the Cf-peptides' uptake was tested under specific experimental conditions: energy (ATP) depletion, endocytic inhibitors, and low temperature. In a preliminary experiment, the *in vitro* cytotoxic effect of the inhibitor compounds was determined on A431 cells using the MTT assay (data are presented in Table S4). The following chemical inhibitor compounds were used: (i) 5-(*N*-ethyl-*N*-isopropyl)-amiloride (EIPA), an amiloride analog, which is a macropinocytosis inhibitor;[45,46] (ii) β-methyl-cyclodextrin (βMCD), which selectively extracts cholesterol from the plasma membrane, thus targeting caveolae and lipid raft internalization pathways;[47] (iii) 2-deoxy-glucose and Na-azide for adenosine-triphosphate (ATP) depletion. The antimetabolite 2-deoxy-glucose inhibits ATP production by glycolysis and Na-azide inhibits oxidative phosphorylation.[48]

Figure 8B−D presents the data obtained from the inhibition studies. All the chemical inhibitors and the low temperature (see the Supporting Information) decreased the cellular uptake of the Cf-peptides (at a concentration of 25 μM). These observations suggest that the Cf-peptides mainly internalize through energy-dependent ways. Moreover, EIPA reduced most of the uptake of Cf peptides; this suggests that macropinocytosis also plays an important role in the internalization of these peptides. We had similar observations in the case of S100A4 peptides.

■ DISCUSSION

We performed an in-depth analysis of water-soluble drug delivery candidate peptides, studying separately the (5)- and (6)-carboxyfluorescein-conjugated isomers. Using an extensive NMR spectroscopic investigation, we showed that the Cf conjugation/modification can influence the structural features of the attached peptide that might alter the cellular uptake and, consequently, the drawn conclusions.

All four peptides are taken up by the A431 cells without any *in vitro* cytotoxic effects. Based on CLSM studies, the Cf peptides have different intracellular localization. Thus, the ERD-A peptide is localized mainly in the cytoplasm, ERD-B
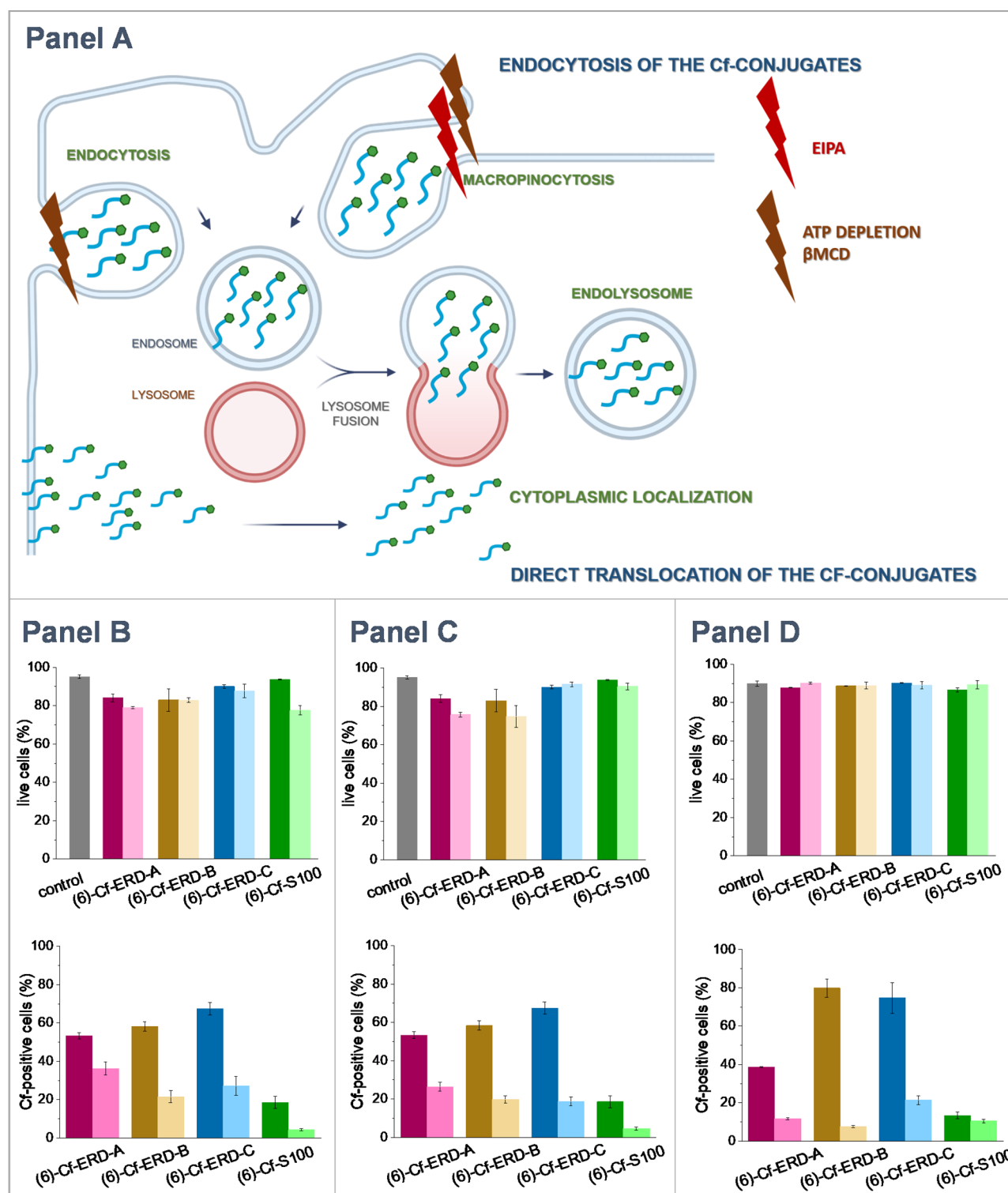
Figure 8. (A) Schematic representation of cellular internalization pathways and their main chemical inhibitors. Effect of chemical endocytosis inhibitors on the cell viability (B, 50 μM EIPA; C, 2 mM βMCD; D, 25 mM 2-deoxy-glucose + 50 μM Na-azide). Upper parts: ratio of living, fluorescence-positive A431 cells (B, 50 μM EIPA; C, 2 mM βMCD; D, 25 mM 2-deoxy-glucose + 50 μM Na-azide). Bottom parts: cellular uptake of the Cf peptides without (deeper color) and with inhibitor compounds; ratio of Cf-positive live cells. Error bars correspond to SEM. The cells were pre-incubated with the inhibitors for 30 min and then treated with the peptides for 90 min at 25 μM.

has partial colocalization with lysosomal staining, and ERD-C is mainly localized in the lysosomes. The S100 peptide also has partial colocalization with lysosomal staining.

The uptake mechanism for all peptides mainly occurs through energy-dependent paths and can be inhibited chemically. At lower concentration endocytosis might be dominant, while Cf-peptide is applied at higher concentration, it translocates directly. The intracellular localization of the Cf-peptides also suggests that once they internalized, they follow mainly endocytic pathways toward late endosomes and

lysosomes and may be degraded within a lysosomal compartment.

However, the cellular uptake was different depending on the constitutional isomerism of Cf. The NMR-based structural characterization of (5)- and (6)-Cf-conjugated peptides showed that in the pH = 3−7 range, the main tautomer of both (5)- and (6)-Cf is the carboxylic acid form. Furthermore, the attached Cf has a long-range effect on the peptide amide environments, which is usually more accentuated for (6)-Cf than (5)-Cf. But these effects do not induce major structural differences. All peptides are disordered with slight helical tendencies in the nonfluorescent form Upon Cf conjugation, ERD-A acquires the strongest helical tendency, while ERD-B and S100 gain only a weaker one; Cf has the least effect on the overall structure of ERD-C. On the other hand, the (5)-Cf peptides have a slightly higher helical tendency than their respective (6)-Cf derivatives.

As the pH is different in the cytoplasm and in the cellular compartments, the pH effect on the structure was studied in the pH = 3−7 range. In this respect, ERD-A shows a slight change, as (5)-Cf-ERD-A is the most helical at pH = 7, but no significant differences for (5)- and (6)-Cf-ERD-B were found.

We found that the peptide amino acid sequence is also important. Cf conjugation causes changes for ERD-A, ERD-B, and S100, where, especially in the N-terminal part, aromatic residues are present, and aromatic and hydrophobic interactions between the sidechain and the Cf moiety are possible. Although no stable secondary structural elements can be found, for most peptides, weak NOE cross-peaks between Cf and the Phe5 residue are detectable (ERD-A, ERD-B, and S100). Regarding Pro environments, due to the occurring *cis/ trans* isomerization, minor forms are present as well, thus conferring an even more heterogeneous ensemble of the system that might affect cell-penetration properties.

The small structural differences resulting from the NMR investigations can influence the cellular uptake, as the order of the uptake tendency is ERD-B > ERD-A > ERD-C > S100. An explanation for this tendency can be the difference in hydrophobicity and the pattern of hydrophobic/hydrophilic residues (see Scheme 1A), the existence and the position of the aromatic residues, and also the *trans/cis*-proline equilibrium that caused increased conformational heterogeneity. The hydrophobicity is similar for all studied peptides, but the less internalized peptide S100 is the most hydrophilic. Here, all hydrophobic aromatic residues are situated at the N-terminus and the Cf conjugation/modification does not change the overall hydrophobicity. The N-termini of ERD peptides are originally hydrophilic and acquire some hydrophobicity upon Cf conjugation. Furthermore, we prove that in the S100 peptide, the Pro6 residue undergoes a *cis/trans* isomerization, altering the overall peptide structure and flexibility. The minor conformer is 25% and the turn in its structure might contribute to the lower cellular internalization, as it can be disadvantageous for receptor binding.[49]

The dehydrin-derived peptides have a similar hydrophobic pattern, but ERD-C contains no aromatic residues. This can be disadvantageous, as the peptide internalizes through ATP-dependent pathways and most receptors have an aromatic binding pocket. This underlines the necessity of including an aromatic residue in a well-designed position. For the studied plant-derived cationic peptides, small changes in the peptide sequence result in remarkable differences in the intracellular fate. This gives an opportunity to fine-tune the intracellular fate.

of a cargo. On the other hand, the human-based S100 C-terminal fragment—contrary to previous literature findings—does not act as a real CPP.

In conclusion, we found that all the studied ERD and S100 peptides are promising tools for cargo delivery for cytoplasmic targets. They all share the advantage of being nontoxic and have no cytostatic effect, and especially, the plant-based fragments can be a safer choice for human applications.

At the same time, we show the wealth of information from a generally applicable in-depth NMR investigation, performed without the need of isotope labeling. This unambiguously determines even small changes in peptide behavior, and measurements can be easily performed for studying the effect of mutations for any other drug carrier candidates and for determining the influence of the fluorescent dye on the peptide structure/behavior. This atomic resolution information can explain and/or help predict drug carrier properties.

■ EXPERIMENTAL SECTION

Materials. 5(6)-Carboxyfluorescein (Cf) was purchased from Acros Organics (Thermo Fisher Scientific, Waltham, MA, USA). TentaGel S Ram resin, 1-hydroxybenzotriazole (HOBT), triisopropylsilane (TIS), and *N,N*′-dicyclohexylcarbodiimide (DCC) were from Sigma-Aldrich. Trifluoroacetic acid (TFA), *N,N*-dimethylformamide (DMF), and 1,4-dithiothreitol (DTT) were purchased from VWR (Budapest, Hungary). All reagents and solvents were of analytical grade or highest available purity and were used without further purification.

For the *in vitro* assays, Roswell Park Memorial Institute 1640 medium (RPMI-1640), Dulbecco's modified Eagle's medium (DMEM), phosphate-buffered saline (PBS), trypan blue, and L-glutamine were from Lonza (Basel, Switzerland). Fetal bovine serum (FBS) was purchased from BioSera (Nuaille, France). Pyruvate, trypsin, 3-(4,5-dimethylthiazol-2-yl)-2,5-diphenyltetrazolium bromide (MTT), paraformaldehyde (PFA), and Mowiol 4−88 were obtained from Sigma-Aldrich. Non-essential amino acids and penicillin/streptomycin (10,000 units penicillin and 10 mg streptomycin/mL) were from Gibco (Thermo Fisher Scientific, Waltham, MA, USA). HPMI buffer (HEPES-buffered medium substitute: 9 mM glucose, 10 mM NaHCO$_3$, 119 mM NaCl, 9 mM HEPES, 5 mM KCl, 0.85 mM MgCl$_2$, 0.053 mM CaCl$_2$, and 5 mM Na$_2$HPO$_4$·2H$_2$O (pH 7.4))[50] was prepared in our laboratory using components obtained from Sigma-Aldrich. Twenty-four- and 96-well cell culture plates and FACS tubes were from Sarstedt (Nümbrecht, Germany). Hoechst 33342 and LysoTracker Deep Red were from Thermo Fisher Scientific. DMSO-d_6 (99.8% purity) and D$_2$O were purchased from EURISOTOP.

Peptide Synthesis. The designed peptides were synthesized using solid-phase peptide synthesis, applying the Fmoc/ *t*Bu strategy using a CEM microwave-assisted fully automated peptide synthesizer. The syntheses were carried out at a 0.25 mmol synthesis scale using a TentaGel S Ram resin with a loading of 0.23 mmol/g amino function. 5(6)-Carboxyfluorescein (3 molar equiv, 0.15 mmol, 56 mg) was conjugated manually to the N-terminus of 0.05 mmol of peptide (297 mg of resin) using HOBT (3 molar equiv, 0.15 mmol, 22.9 mg) and DCC (3 molar equiv, 0.15 mmol, 30.9 mg) in DMF using double coupling at room temperature overnight. The Cf peptides were detached from the solid support using TFA (90%) in the presence of water (5%), 1,4-dithiothreitol (DTT, 2.5%), and TIS (2.5%). The cleaved peptides were analyzed by

RP-HPLC/MS (A: 0.1% TFA; B: 80% AcN/water) on a PerfectSil 100 ODS-3 5 μm column (250 × 4.6 mm), with a flow of 1 mL/min.

Purification of Crude Peptides. The crude Cf peptides were purified using a C18 RP-HPLC on a PerfectSil 100 ODS-3 5 μm column (250 × 10 mm). All compounds are >95% pure by HPLC analysis. In most cases, the two regioisomers (5)-Cf and (6)-Cf were well separable on the RP-HPLC column (100% purity of the given isomer confirmed by NMR); only for ERD-B, an isomeric ratio of 80:20 could be achieved during purification.

The mass accuracy of the products was determined by ESI-MS using a Waters SQ detector (Milford, MA, USA). The mass spectra were recorded in positive ion mode in the 200.0−3000.0 m/z range.

Determination of the Lipophilicity Profile of the Peptides and Their Cf Conjugates. To compare and estimate the lipophilicity of the peptides and Cf peptides, their retention times were determined under the same conditions (HPLC system, column, gradient, and eluent composition). As these compounds are structurally similar, their retention times can serve as a basis to compare the lipophilicity of compounds.[35,51−53] The more lipophilic a compound, the higher its retention on the nonpolar stationary phase. Log$P$ values were also calculated with the Chemicalize online platform (https://chemicalize.com/app/calculation, ChemAxonPASS)[54−57] using the PhysProp database[58] (available from Syracuse Research Corporation; Physical/Chemical Property Database (PHYSPROP); SRC Environmental Science Center: Syracuse, NY, 1994) and the ChemAxon and Klopman *et al.* models.[54,55]

NMR Experiments and Data Analysis. Typical NMR samples contained 1 mM peptides or Cf-peptide derivatives, 450 μL of H_2O, and 50 μL of D_2O. In the case of pH dependency, the pH was adjusted with NaOH or HCl. The two Cf samples were prepared: both contained 1 mM 5(6)-carboxyfluorescein; in the first case, the solvent was 600 μL of DMSO-d_6, and for the second sample, Cf was dissolved in 450 μL of 0.1 M NaOH and 50 μL of D_2O.

All NMR spectra were recorded on a Bruker Avance III 700 spectrometer (700.05 MHz for ^{1}H; 70.94 MHz for ^{15}N; 176.03 MHz for ^{13}C) using a Prodigy TCI H&F-C/N-D, 5 mm z-gradient probehead. The temperature was calibrated against the methanol standard sample; measurements were performed at 298 K. ^{1}H chemical shifts were referenced to the internal DSS standard. Resonance assignment and sequential connectivities for peptides, Cf-conjugated peptides, and Cf samples were determined from 2D homonuclear ^{1}H,^{1}H-TOCSY (mixing time, 80 ms) and ^{1}H,^{1}H-NOESY (mixing time, 300 ms) measurements. ^{1}H,^{15}N SOFAST-HMQC, ^{1}H,^{13}C-HSQC, and ^{1}H,^{13}C-HMBC for all samples were performed on the natural abundance compounds. All spectra were processed in TopSpin 3.6.0. Peak assignment was done using Sparky.[59]

NMR Chemical Shifts. 5(6)-Carboxyfluorescein ^{1}H NMR (700 MHz, DMSO-d_6) δ/ppm 10.26 (s, 4H), 8.49 (dd, J = 0.7 Hz, 1H), 8.40 (dd, 1H), 8.32 (dd, 1H), 8.21 (dd, 1H), 7.75 (m, 1H), 7.50 (dd, 1H), 6.79 (m, 4H), 6.71 (d, J = 6.1 Hz, 2H), 6.70 (d, J = 6.1 Hz, 2H), 6.66 (m, 2H), 6.64 (m, 2H).

^{1}H NMR (700 MHz, 450 μL of 0.025 M NaOH and 50 μL of D_2O) δ/ppm 8.26 (d, J = 1.7 Hz, 1H), 8.06 (m, 2H), 7.86 (d, J = 8.27 Hz, 1H), 7.76 (d, 1.60 Hz, 1H), 7.39 (d, J = 8.1 Hz, 1H), 7.21 (d, J = 9.3 Hz, 4H), 6.64 (m, 8H).

Fluorescence Properties of 5(6)-Carboxyfluorescein-Peptide Derivatives. The pH dependence of the Cf-peptide derivatives was tested as described in ref.[35] Briefly, peptide stock solutions (concentration: 625 μM) were prepared by dissolving peptides in DMSO. Solutions with different pH values were prepared by mixing 0.1 M citric acid and 0.2 M disodium phosphate (Na_2HPO_4) buffers at a defined ratio: 12.29 mL of citric acid and 7.71 mL of Na_2HPO_4 for pH 4.0; 9.70 mL of citric acid and 10.30 mL of Na_2HPO_4 for pH 5.0; 7.37 mL of citric acid and 12.63 mL of Na_2HPO_4 for pH 6.0; 3.54 mL of citric acid and 16.47 mL of Na_2HPO_4 for pH 7.0; 1.27 mL of citric acid and 18.27 mL of Na_2HPO_4 for pH 7.6.

Thirty microliters of peptide stock solution was added to 2970 μL of buffer solution (concentration: 6.25 μM). Fluorescence intensity was determined using a Varian Cary Eclipse spectrofluorometer (Agilent Technologies, Santa Clara, CA, USA). The following settings were used: excitation: λ = 488 nm; emission: λ = 490−700 nm; detector voltage: 450 V (in the case of (6)-Cf-ERD-C, also 400 V detector voltage was applied).[35]

Cell Culturing. MonoMac6 human monocytic leukemia cells[60] (DSMZ no.: ACC 124, Deutsche Sammlung von Mikroorganismen and Zellkulturen GmbH, Braunschweig, Germany) and A431 human skin squamous cell carcinoma cells[61] (ATCC CRL-1555, American Type Culture Collection) were used for the *in vitro* evaluation studies. For maintaining MonoMac6 cell culture, RPMI-1640 medium supplemented with 10% heat-inactivated FBS, 2 mM L-glutamine, and 100 μg/mL penicillin/streptomycin was used; in the case of A431 cell culture, DMEM supplemented with 10% heat-inactivated FBS, 2 mM L-glutamine, 100 μg/mL penicillin/streptomycin, 1 mM pyruvate, and 1% non-essential amino acids (DMEM CM) was used. Cells were incubated at 37 °C in a humified atmosphere with 5% CO_2.

Determination of *In Vitro* Cytostatic and Cytotoxic Effects. The *in vitro* cytostatic effect of peptides was determined on A431 cells using the MTT assay. Cells were seeded during the exponential growth phase on a standard 96-well cell culture plate in a density of 5 × 10^3 cells/100 μL/well 1 day prior the experiment. Cells were treated with the compounds dissolved in incomplete medium (ICM) with 10% (v/v) distilled water in the concentration range of 1.28 × 10^{-3} to 100 μM. Cells were treated with the compounds for 20−24 h. As controls, ICM and ICM containing 10% (v/v) distilled water were used.

The cytotoxic effect of cellular uptake inhibitor compounds on A431 cells was also studied. In this case, 15 × 10^3 cells/100 μL/well density was used, and treatment was in the following concentration ranges: 4−1000 μM EIPA and 200 μM to 50 mM βMCD; ATP depletion: 240−6000 μM 2-deoxy-glucose and 0.4−100 μM Na-azide for 3 h.

After the treatment, cells were washed three times with ICM. In the last step of cytostasis study, DMEM CM was added, and cells were cultured for 72 h. After culturing the cells or immediately after washing, 45 μL of sterile-filtered MTT (3-(4,5-dimethylthiazol-2-yl)-2,5-diphenyltetrazolium bromide) was added (2 mg/mL) to the cells. Mitochondrial enzymes reduce MTT to a formazan derivative (purple crystals).[62−64]

After 3.5 h of incubation, plates were centrifuged (2000 rpm, 5 min), the supernatant was removed, and formazan crystals were dissolved in DMSO. The absorbance was determined with an ELISA plate reader (Labsystems iEMS reader, Helsinki, Finland) at λ = 540 and 620 nm. A_{620} values were

subtracted from A_{540} values, and cytostatic or cytotoxic activity was calculated with the formula cytostasis% = $100 \times (1 - A_{\text{treated cells}}/A_{\text{control cells}})$, where $A_{\text{treated cells}}$ and $A_{\text{control cells}}$ are the average absorbance of treated and control cells, respectively. The 50% inhibitory concentration (IC_{50}) values were determined from the dose−response curves. The curves were calculated with Microcal OriginPro (version: 2018) software.

Determination of *In Vitro* Cellular Uptake. For the *in vitro* cellular uptake studies, a BD LSR II (BD Biosciences, San Jose, CA, USA) flow cytometer was used. The *in vitro* cellular uptake of Cf peptides was determined on MonoMac6 and A431 cells. Cells were seeded during the exponential growth phase 1 day prior to the experiment to 24-well cell culture plates with a density of 10^5 cells/1 mL/well. Dilution series were prepared in RPMI-1640 or DMEM ICM with 10% distilled water (v/v) in the concentration range of 6.25−50 or 0.2−25 μM. Cells were treated with the Cf peptides for 30 min, 1.5 h, and 3 h, and then, they were washed once with RPMI-1640 or DMEM ICM and once with HPMI. To remove the surface-bound peptides and detach cells from the plate, 100 μL of trypsin was added to the cells for 2 or 4 min in the case of MonoMac6 and for 4 or 8 min in the case of A431 cells. Trypsin activity was stopped with 800 μL of HPMI medium supplemented with 10% FBS. Cells were then transferred into FACS tubes and centrifuged (5 min, 1000 rpm), and after removing the supernatant, 300 μL of HPMI was added. The intracellular fluorescence intensity of cells was measured at λ_{ex} = 488 nm (Coherent Sapphire laser excitation; emission channel: LP 510, BP 530/30). Results were analyzed with FACSDiva 5.0 software.

UC_{50} values, the interpolated concentration required for intracellular fluorescence in 50% of the cells, were calculated as described.[36]

To investigate the mechanism of the cellular uptake, inhibition studies were performed. A431 cells were treated with inhibitor compounds: 50 μM EIPA and 2 mM βMCD; ATP depletion: 25 mM 2-deoxy-glucose and 50 μM Na-azide for 60 min. After incubation with the inhibitors, Cf peptides were added to the cells with a final concentration of 25 μM. Also, cellular uptake at 4 °C was determined at 12.5 and 25 μM. Cells were treated with the Cf peptides for 90 min. As controls, cells without inhibitor compounds were used. After the treatment, cells were washed and trypsinized. Cells were transferred to FACS tubes and flow cytometry measurement was performed using a BD LSR II flow cytometer as described above.

***In Vitro* Intracellular Localization Using Confocal Laser Scanning Microscopy.** A431 cells were seeded in complete cell medium to 24-well cell culture plates at a density of 10^5 cells/1 mL/well, which contained cover glasses (thickness 1, Assistant, Karl Hecht GmbH and Co KG, Sondheim/Rhön, Germany), 24 h before the experiment. Cells were treated with the Cf peptides (concentration: 25 μM) for 90 min in DMEM ICM with 10% distilled water (v/v). Lysosomes were stained with LysoTracker Deep Red, and nuclei were stained with Hoechst 33342, according to the manufacturer's suggestions. After each step, cells were washed three times with ICM. Cells were fixed with 4% PFA for 20 min at 37 °C. After washing three times with PBS, cover glasses were mounted to microscopy slides (VWR) by Mowiol 4−88 mounting medium.

CLSM studies were performed on a Zeiss LSM 710 system (Carl Zeiss Microscopy GmbH, Jena, Germany) with a 40×/

1.4 Plan-Apochromat oil immersion objective with the following parameters: Cf-peptides: λ_{ex} = 488 nm, λ_{em} = 541 nm; nuclei: λ_{ex} = 405 nm, λ_{em} = 467 nm (Hoechst 33342); lysosomes: λ_{ex} = 633 nm, λ_{em} = 720 nm (LysoTracker Deep Red). Zeiss ZEN lite software (Carl Zeiss Microscopy GmbH) was used for image processing. Line scan analysis was performed by National Institutes of Health (NIH) ImageJ software using the Plot Profile application. On grayscale images, lines (width: 50) were drawn starting from the cell nucleus toward the cytoplasm. The obtained gray values correspond to the intensity of a given pixel on a scale of 0 to 255. All line scan lengths were normalized to 1, yielding a normalized diameter, and the line scans were plotted using Microcal OriginPro (version: 2018) software.

■ ASSOCIATED CONTENT

Ⓢ Supporting Information

The Supporting Information is available free of charge at https://pubs.acs.org/doi/10.1021/acsomega.1c04637.

> MS, analytical HPLC chromatograms, fluorescence intensity studies, NMR studies, additional *in vitro* cellular internalization and confocal microscopy studies, inhibition of cellular uptake (PDF)
>
> Molecular formula strings (XLSX)

■ AUTHOR INFORMATION

Corresponding Author

Andrea Bodor − *Institute of Chemistry, ELTE−Eötvös Loránd University, H-1117 Budapest, Hungary;* ⓞ orcid.org/0000-0002-7422-298X; Email: andrea.bodor@ttk.elte.hu

Authors

Fanni Sebák − *Institute of Chemistry, ELTE−Eötvös Loránd University, H-1117 Budapest, Hungary; Doctoral School of Pharmaceutical Sciences, Semmelweis University, H-1085 Budapest, Hungary*

Lilla Borbála Horváth − *ELKH-ELTE Research Group of Peptide Chemistry, Eötvös Loránd Research Network, Eötvös Loránd University, H-1117 Budapest, Hungary; National Public Health Center, Budapest H-1097, Hungary; Hevesy György PhD School of Chemistry, ELTE Eötvös Loránd University, H-1117 Budapest, Hungary*

Dániel Kovács − *Institute of Chemistry, ELTE−Eötvös Loránd University, H-1117 Budapest, Hungary; Hevesy György PhD School of Chemistry, ELTE Eötvös Loránd University, H-1117 Budapest, Hungary*

János Szolomájer − *Department of Medical Chemistry, University of Szeged, H-6720 Szeged, Hungary*

Gábor K. Tóth − *Department of Medical Chemistry, University of Szeged, H-6720 Szeged, Hungary*

Ákos Babiczky − *Institute of Cognitive Neuroscience and Psychology, Research Centre for Natural Sciences, H-1117 Budapest, Hungary; Doctoral School of Psychology/Cognitive Science, Budapest University of Technology and Economics, H-1111 Budapest, Hungary*

Szilvia Bősze − *ELKH-ELTE Research Group of Peptide Chemistry, Eötvös Loránd Research Network, Eötvös Loránd University, H-1117 Budapest, Hungary; National Public Health Center, Budapest H-1097, Hungary*

Complete contact information is available at:
https://pubs.acs.org/10.1021/acsomega.1c04637

Author Contributions

The manuscript was written through contributions of all authors. All authors have given approval to the final version of the manuscript.

Notes

The authors declare no competing financial interest.
NMR assignment data have been deposited in BMRB with the following accession numbers: ERD-A: 51040; ERD-B: 51039; ERD-C: 51041; S100: 51042.

■ ABBREVIATIONS

βMCD, β-methyl-cyclodextrin; AcN, acetonitrile; ATCC, American Type Culture Collection; ATP, adenosine triphosphate; CD, circular dichroism; Cf, 5(6)-carboxyfluorescein; CLSM, confocal laser scanning microscopy; CM, complete medium; CPP, cell-penetrating peptide; DCC, N,N'-dicyclohexylcarbodiimide; DMEM, Dulbecco's modified Eagle's medium; DMF, N,N-dimethylformamide; DMSO, dimethyl sulfoxide; DSMZ, Deutsche Sammlung von Mikroorganismen und Zellkulturen; DTT, 1,4-dithiothreitol; EIPA, 5-(N-ethyl-N-isopropyl)-amiloride; ERD-A, ERD14 K segment A; ERD-B, ERD14 K segment B; ERD-C, ERD14 K segment C; FBS, fetal bovine serum; Fmoc, 9-fluorenylmethyloxycarbonyl; HMBC, heteronuclear multiple bond correlation; HSQC, heteronuclear single quantum coherence; HOBT, 1-hydroxybenzotriazole; ICM, incomplete medium; MTT, 3-(4,5-dimethylthiazol-2-yl)-2,5-diphenyltetrazolium bromide; NIH, National Institutes of Health; NMP, 1-methyl-2-pyrrolidone; NMR, nuclear magnetic resonance; NOE, nuclear Overhauser effect; NOESY, nuclear Overhauser effect spectroscopy; PBS, phosphate-buffered saline; PFA, paraformaldehyde; RCCS, random coil chemical shift; RP-HPLC, reverse-phase high-performance liquid chromatography; RPMI-1640, Roswell Park Memorial Institute 1640 medium; Rt, retention time; S100, C-terminal region of S100A4 protein; SCS, secondary chemical shift; SEM, standard error of the mean; SOFAST-HMQC, band-selective optimized flip angle short transient heteronuclear multiple-quantum correlation; TFA, trifluoracetic acid; TIS, triisopropylsilane

■ REFERENCES

(1) Green, M.; Loewenstein, P. M. Autonomous functional domains of chemically synthesized human immunodeficiency virus tat trans-activator protein. *Cell* **1988**, *55*, 1179−1188.

(2) Vivès, E.; Brodin, P.; Lebleu, B. A truncated HIV-1 Tat protein basic domain rapidly translocates through the plasma membrane and accumulates in the cell nucleus. *J. Biol. Chem.* **1997**, *272*, 16010−16017.

(3) Joliot, A.; Pernelle, C.; Deagostini-Bazin, H.; Prochiantz, A. Antennapedia homeobox peptide regulates neural morphogenesis. *Proc. Natl. Acad. Sci. U. S. A.* **1991**, *88*, 1864−1868.

(4) Derossi, D.; Calvet, S.; Trembleau, A.; Brunissen, A.; Chassaing, G.; Prochiantz, A. Cell internalization of the third helix of the Antennapedia homeodomain is receptor-independent. *J. Biol. Chem.* **1996**, *271*, 18188−18193.

(5) El-Andaloussi, S.; Järver, P.; Johansson, H. J.; Langel, Ü. Cargo-dependent cytotoxicity and delivery efficacy of cell-penetrating peptides: a comparative study. *Biochem. J.* **2007**, *407*, 285−292.

(6) De Coninck, B.; De Smet, I. Plant peptides - taking them to the next level. *J. Exp. Bot.* **2016**, *67*, 4791−4795.

(7) Apone, F.; Barbulova, A.; Colucci, M. G. Plant and Microalgae Derived Peptides Are Advantageously Employed as Bioactive Compounds in Cosmetics. *Front. Plant Sci.* **2019**, *10*, 756.

(8) Das, D.; Jaiswal, M.; Khan, F. N.; Ahamad, S.; Kumar, S. PlantPepDB: A manually curated plant peptide database. *Sci. Rep.* **2020**, *10*, 2194.

(9) Kovacs, D.; Kalmar, E.; Torok, Z.; Tompa, P. Chaperone activity of ERD10 and ERD14, two disordered stress-related plant proteins. *Plant Physiol.* **2008**, *147*, 381−390.

(10) Atkinson, J.; Clarke, M. W.; Warnica, J. M.; Boddington, K. F.; Graether, S. P. Structure of an Intrinsically Disordered Stress Protein Alone and Bound to a Membrane Surface. *Biophys. J.* **2016**, *111*, 480−491.

(11) Graether, S. P.; Boddington, K. F. Disorder and function: a review of the dehydrin protein family. *Front. Plant Sci.* **2014**, *5*, 576.

(12) Koag, M. C.; Wilkens, S.; Fenton, R. D.; Resnik, J.; Vo, E.; Close, T. J. The K-segment of maize DHN1 mediates binding to anionic phospholipid vesicles and concomitant structural changes. *Plant Physiol.* **2009**, *150*, 1503−1514.

(13) Eriksson, S. K.; Kutzer, M.; Procek, J.; Gröbner, G.; Harryson, P. Tunable membrane binding of the intrinsically disordered dehydrin Lti30, a cold-induced plant stress protein. *Plant Cell* **2011**, *23*, 2391−2404.

(14) Murvai, N.; Kalmar, L.; Szalaine Agoston, B.; Szabo, B.; Tantos, A.; Csikos, G.; Micsonai, A.; Kardos, J.; Vertommen, D.; Nguyen, P. N.; Hristozova, N.; Lang, A.; Kovacs, D.; Buday, L.; Han, K. H.; Perczel, A.; Tompa, P. Interplay of Structural Disorder and Short Binding Elements in the Cellular Chaperone Function of Plant Dehydrin ERD14. *Cell* **2020**, *9*, 1856.

(15) Murvai, N.; Kalmar, L.; Szabo, B.; Schad, E.; Micsonai, A.; Kardos, J.; Buday, L.; Han, K. H.; Tompa, P.; Tantos, A. Cellular Chaperone Function of Intrinsically Disordered Dehydrin ERD14. *Int. J. Mol. Sci.* **2021**, *22*, 6190.

(16) Fei, F.; Qu, J.; Zhang, M.; Li, Y.; Zhang, S. S100A4 in cancer progression and metastasis: A systematic review. *Oncotarget* **2017**, *8*, 73219−73239.

(17) Nader, J. S.; Guillon, J.; Petit, C.; Boissard, A.; Franconi, F.; Blandin, S.; Lambot, S.; Grégoire, M.; Verrièle, V.; Nawrocki-Raby, B.; Birembaut, P.; Coqueret, O.; Guette, C.; Pouliquen, D. L. S100A4 is a Biomarker of Tumorigenesis, EMT, Invasion, and Colonization of Host Organs in Experimental Malignant Mesothelioma. *Cancers* **2020**, *12*, 939.

(18) Zhang, S.; Wang, G.; Liu, D.; Bao, Z.; Fernig, D. G.; Rudland, P. S.; Barraclough, R. The C-terminal region of S100A4 is important for its metastasis-inducing properties. *Oncogene* **2005**, *24*, 4401−4411.

(19) Malashkevich, V. N.; Varney, K. M.; Garrett, S. C.; Wilder, P. T.; Knight, D.; Charpentier, T. H.; Ramagopal, U. A.; Almo, S. C.; Weber, D. J.; Bresnick, A. R. Structure of Ca2+−bound S100A4 and its interaction with peptides derived from nonmuscle myosin-IIA. *Biochemistry* **2008**, *47*, 5111−5126.

(20) Biri-Kovács, B.; Kiss, B.; Vadászi, H.; Gógl, G.; Pálfy, G.; Török, G.; Homolya, L.; Bodor, A.; Nyitray, L. Ezrin interacts with S100A4 via both its N- and C-terminal domains. *PLoS One* **2017**, *12*, No. e0177489.

(21) Jones, A. T.; Sayers, E. J. Cell entry of cell penetrating peptides: tales of tails wagging dogs. *J. Controlled Release* **2012**, *161*, 582−591.

(22) Wei, L.; Tang, J.; Zou, Q. SkipCPP-Pred: an improved and promising sequence-based predictor for predicting cell-penetrating peptides. *BMC Genomics* **2017**, *18*, 742.

(23) Lavis, L. D. Teaching Old Dyes New Tricks: Biological Probes Built from Fluoresceins and Rhodamines. *Annu. Rev. Biochem.* **2017**, *86*, 825−843.

(24) Fischer, R.; Mader, O.; Jung, G.; Brock, R. Extending the applicability of carboxyfluorescein in solid-phase synthesis. *Bioconjugate Chem.* **2003**, *14*, 653−660.

(25) Kiss, É.; Gyulai, G.; Pári, E.; Horváti, K.; Bősze, S. Membrane affinity and fluorescent labelling: comparative study of monolayer interaction, cellular uptake and cytotoxicity profile of carboxyfluorescein-conjugated cationic peptides. *Amino Acids* **2018**, *50*, 1557−1571.

(26) Szeto, H. H.; Schiller, P. W.; Zhao, K.; Luo, G. Fluorescent dyes alter intracellular targeting and function of cell-penetrating tetrapeptides. *FASEB J.* **2005**, *19*, 118−120.

(27) Cardozo, A. K.; Buchillier, V.; Mathieu, M.; Chen, J.; Ortis, F.; Ladrière, L.; Allaman-Pillet, N.; Poirot, O.; Kellenberger, S.; Beckmann, J. S.; Eizirik, D. L.; Bonny, C.; Maurer, F. Cell-permeable peptides induce dose- and length-dependent cytotoxic effects. *Biochim. Biophys. Acta* **2007**, *1768*, 2222−2234.

(28) Birch, D.; Christensen, M. V.; Staerk, D.; Franzyk, H.; Nielsen, H. M. Fluorophore labeling of a cell-penetrating peptide induces differential effects on its cellular distribution and affects cell viability. *Biochim. Biophys. Acta, Biomembr.* **2017**, *1859*, 2483−2494.

(29) Cavaco, M.; Pérez-Peinado, C.; Valle, J.; Silva, R. D. M.; Correia, J. D. G.; Andreu, D.; Castanho, M. A. R. B.; Neves, V. To What Extent Do Fluorophores Bias the Biological Activity of Peptides? A Practical Approach Using Membrane-Active Peptides as Models. *Front. Bioeng. Biotechnol.* **2020**, *8*, 552035.

(30) Hughes, L. D.; Rawle, R. J.; Boxer, S. G. Choose your label wisely: water-soluble fluorophores often interact with lipid bilayers. *PLoS One* **2014**, *9*, No. e87649.

(31) Bertrand, J. R.; Malvy, C.; Auguste, T.; Tóth, G. K.; Kiss-Ivánkovits, O.; Illyés, E.; Hollósi, M.; Bottka, S.; Laczkó, I. Synthesis and studies on cell-penetrating peptides. *Bioconjugate Chem.* **2009**, *20*, 1307−1314.

(32) Hedegaard, S. F.; Derbas, M. S.; Lind, T. K.; Kasimova, M. R.; Christensen, M. V.; Michaelsen, M. H.; Campbell, R. A.; Jorgensen, L.; Franzyk, H.; Cárdenas, M.; Nielsen, H. M. Fluorophore labeling of a cell-penetrating peptide significantly alters the mode and degree of biomembrane interaction. *Sci. Rep.* **2018**, *8*, 6327.

(33) Orndorff, W. R.; Hemmer, A. J. Fluorescein and some of its derivatives. *J. Am. Chem. Soc.* **1927**, *49*, 1272−1280.

(34) Romanchuk, K. G. Fluorescein. Physiochemical factors affecting its fluorescence. *Surv. Ophthalmol.* **1982**, *26*, 269−283.

(35) Baranyai, Z.; Krátký, M.; Vosátka, R.; Szabó, E.; Senoner, Z.; Dávid, S.; Stolaříková, J.; Vinšová, J.; Bősze, S. In vitro biological evaluation of new antimycobacterial salicylanilide-tuftsin conjugates. *Eur. J. Med. Chem.* **2017**, *133*, 152−173.

(36) Bősze, S.; Zsila, F.; Biri-Kovács, B.; Szeder, B.; Majer, Z.; Hudecz, F.; Uray, K. Tailoring Uptake Efficacy of HSV-1 gD Derived Carrier Peptides. *Biomolecules* **2020**, 721.

(37) Schanda, P.; Brutscher, B. Very fast two-dimensional NMR spectroscopy for real-time investigation of dynamic events in proteins on the time scale of seconds. *J. Am. Chem. Soc.* **2005**, *127*, 8014−8015.

(38) Pálfy, G.; Kiss, B.; Nyitray, L.; Bodor, A. Multilevel Changes in Protein Dynamics upon Complex Formation of the Calcium-Loaded S100A4 with a Nonmuscle Myosin IIA Tail Fragment. *ChemBioChem* **2016**, *17*, 1829−1838.

(39) Nielsen, J. T.; Mulder, F. A. A. POTENCI: prediction of temperature, neighbor and pH-corrected chemical shifts for intrinsically disordered proteins. *J. Biomol. NMR* **2018**, *70*, 141−165.

(40) Alderson, T. R.; Lee, J. H.; Charlier, C.; Ying, J.; Bax, A. Propensity for cis-Proline Formation in Unfolded Proteins. *ChemBioChem* **2018**, *19*, 37−42.

(41) Sebák, F.; Ecsédi, P.; Bermel, W.; Luy, B.; Nyitray, L.; Bodor, A. Selective 1Hα NMR methods to reveal functionally relevant proline cis/trans isomers in IDPs: characterization of minor forms, effects of phosphorylation and occurrence in proteome. *Angew. Chem.-Int. Edit.* **2021** DOI: 10.1002/anie.202108361

(42) Schubert, M.; Labudde, D.; Oschkinat, H.; Schmieder, P. A software tool for the prediction of Xaa-Pro peptide bond conformations in proteins based on C-13 chemical shift statistics. *J. Biomol. NMR* **2002**, *24*, 149−154.

(43) Trabulo, S.; Cardoso, A. L.; Mano, M.; De Lima, M. C. P. Cell-Penetrating Peptides-Mechanisms of Cellular Uptake and Generation of Delivery Systems. *Pharmaceuticals* **2010**, *3*, 961−993.

(44) Conner, S. D.; Schmid, S. L. Regulated portals of entry into the cell. *Nature* **2003**, *422*, 37−44.

(45) Swanson, J. A.; Watts, C. Macropinocytosis. *Trends Cell Biol.* **1995**, *5*, 424−428.

(46) Meier, O.; Boucke, K.; Hammer, S. V.; Keller, S.; Stidwill, R. P.; Hemmi, S.; Greber, U. F. Adenovirus triggers macropinocytosis and endosomal leakage together with its clathrin-mediated uptake. *J. Cell Biol.* **2002**, *158*, 1119−1131.

(47) Rodal, S. K.; Skretting, G.; Garred, Ø.; Vilhardt, F.; van Deurs, B.; Sandvig, K. Extraction of cholesterol with methyl-beta-cyclodextrin perturbs formation of clathrin-coated endocytic vesicles. *Mol. Biol. Cell* **1999**, *10*, 961−974.

(48) Schwoebel, E. D.; Ho, T. H.; Moore, M. S. The mechanism of inhibition of Ran-dependent nuclear transport by cellular ATP depletion. *J. Cell Biol.* **2002**, *157*, 963−974.

(49) Craveur, P.; Joseph, A. P.; Poulain, P.; de Brevern, A. G.; Rebehmed, J. Cis-trans isomerization of omega dihedrals in proteins. *Amino Acids* **2013**, *45*, 279−289.

(50) Kapus, A.; Grinstein, S.; Wasan, S.; Kandasamy, R.; Orlowski, J. Functional characterization of three isoforms of the Na+/H+ exchanger stably expressed in Chinese hamster ovary cells. ATP dependence, osmotic sensitivity, and role in cell proliferation. *J. Biol. Chem.* **1994**, *269*, 23544−23552.

(51) Rutkowska, E.; Pajak, K.; Jóźwiak, K. Lipophilicity–methods of determination and its role in medicinal chemistry. *Acta Pol. Pharm.* **2013**, *70*, 3−18.

(52) Fernández-Llamazares, A. I.; Adan, J.; Mitjans, F.; Spengler, J.; Albericio, F. Tackling lipophilicity of peptide drugs: replacement of the backbone N-methyl group of cilengitide by N-oligoethylene glycol (N-OEG) chains. *Bioconjugate Chem.* **2014**, *25*, 11−17.

(53) Valkó, K. Application of high-performance liquid chromatography based measurements of lipophilicity to model biological distribution. *J. Chromatogr. A* **2004**, *1037*, 299−310.

(54) Viswanadhan, V. N.; Ghose, A. K.; Revankar, G. R.; Robins, R. K. Atomic physicochemical parameters for three dimensional structure directed quantitative structure-activity relationships. 4. Additional parameters for hydrophobic and dispersive interactions and their application for an automated superposition of certain naturally occurring nucleoside antibiotics. *J. Chem. Inf. Comp. Sci.* **1989**, *29*, 163−172.

(55) Klopman, G.; Li, J.-Y.; Wang, S.; Dimayuga, M. Computer Automated log P Calculations Based on an Extended Group Contribution Approach. *J. Chem. Inf. Comp. Sci.* **1994**, *34*, 752−781.

(56) Csizmadia, F.; Tsantili-Kakoulidou, A.; Panderi, I.; Darvas, F. Prediction of Distribution Coefficient from Structure. 1. Estimation Method. *J. Pharm. Sci.* **1997**, *86*, 865−871.

(57) Bouchard, G.; Carrupt, P. A.; Testa, B.; Gobry, V.; Girault, H. H. The apparent lipophilicity of quaternary ammonium ions is influenced by galvani potential difference, not ion-pairing: a cyclic voltammetry study. *Pharm. Res.* **2001**, *18*, 702−708.

(58) Rosenberg, S. A.; Hueber, A. E.; Aronson, D.; Gouchie, S.; Howard, P.; Meylan, W. M.; Tunkel, J. L. Syracuse research corporation's chemical information databases: Extraction and compilation of data related to environmental fate and exposure. *Sci. Technol. Libr.* **2003**, *23*, 73−87.

(59) Goddard, T. D.; Kneller, D. G. *SPARKY* 3; University of California: San Francisco, 2000.

(60) Ziegler-Heitbroc, H. W. L.; Thiel, E.; Futterer, A.; Herzog, V.; Wirtz, A.; Riethmüller, G. Establishment of a human cell line (Mono Mac 6) with characteristics of mature monocytes. *Int. J. Cancer* **1988**, *41*, 456−461.

(61) Giard, D. J.; Aaronson, S. A.; Todaro, G. J.; Arnstein, P.; Kersey, J. H.; Dosik, H.; Parks, W. P. In vitro cultivation of human tumors: establishment of cell lines derived from a series of solid tumors. *J. Natl. Cancer Inst.* **1973**, *51*, 1417−1423.

(62) Mosmann, T. Rapid colorimetric assay for cellular growth and survival: application to proliferation and cytotoxicity assays. *J. Immunol. Methods* **1983**, *65*, 55−63.

(63) Slater, T. F.; Sawyer, B.; Sträuli, U. Studies on succinate-tetrazolium reductase systems. III. Points of coupling of four different tetrazolium salts. *Biochim. Biophys. Acta* **1963**, *77*, 383−393.

(64) Liu, Y.; Peterson, D. A.; Kimura, H.; Schubert, D. Mechanism of cellular 3-(4,5-dimethylthiazol-2-yl)-2,5-diphenyltetrazolium bromide (MTT) reduction. *J. Neurochem.* **1997**, *69*, 581−593.